SANDIA REPORT

SAND2003-3040
Unlimited Release
Printed August 2003

Calculations of Precursor Propagation in Dispersive Dielectrics

Larry D. Bacon

Prepared by
Sandia National Laboratories
Albuquerque, New Mexico 87185 and Livermore, California 94550

Sandia is a multiprogram laboratory operated by Sandia Corporation,
a Lockheed Martin Company, for the United States Department of Energy's
National Nuclear Security Administration under Contract DE-AC04-94AL85000.

This work was supported by AFOSR under SNL Proposal Number 153020422.

Issued by Sandia National Laboratories, operated for the United States Department of Energy by Sandia Corporation.

Available to DOE and DOE contractors from
U.S. Department of Energy
Office of Scientific and Technical Information
P.O. Box 62
Oak Ridge, TN 37831

Telephone: (865)576-8401
Facsimile: (865)576-5728
E-Mail: reports@adonis.osti.gov
Online ordering: http://www.doe.gov/bridge

Available to the public from
U.S. Department of Commerce
National Technical Information Service
5285 Port Royal Rd
Springfield, VA 22161

Telephone: (800)553-6847
Facsimile: (703)605-6900
E-Mail: orders@ntis.fedworld.gov
Online order: http://www.ntis.gov/help/ordermethods.asp?loc=7-4-0#online

SAND2003-3040
Unlimited Release
Printed August 2003

Calculations of Precursor Propagation in Dispersive Dielectrics

Larry D. Bacon
Directed Energy Special Applications Department
Sandia National Laboratories
P. O. Box 5800
Albuquerque, NM 87185-1153

Abstract

The present study is a numerical investigation of the propagation of electromagnetic transients in dispersive media. It considers propagation in water using Debye and composite Rocard-Powles-Lorentz models for the complex permittivity. The study addresses this question: For practical transmitted spectra, does precursor propagation provide any features that can be used to advantage over conventional signal propagation in models of dispersive media of interest? A companion experimental study is currently in progress that will attempt to measure the effects studied here.

Intentionally Left Blank

CONTENTS

Intentionally Left Blank

1.0 INTRODUCTION

Asymptotic analysis of pulsed electromagnetic wave propagation in dispersive media using the Lorentz model has shown that precursors propagate through the media with a rate of decay of peak amplitude and energy density that is algebraic rather than exponential (Oughstun and Sherman 1994). This could have important implications in the choice of signal waveforms for applications such as ground-penetrating radar (Brock and Patitz 1993) and foliage-penetrating radar (Loubriel, Zutavern et al. 1994). Roberts (2002) has cautioned, however, that this algebraic decay can be observed only for signals that have spectral energy content near zero frequency, which, of course, cannot be radiated efficiently from small platforms. His numerical examples, however, are potentially obscured by the use of ideal, non-causal frequency domain filters. The filters themselves exhibit precursors that can obscure the precursors due to the medium.

The present study is a numerical investigation of the propagation of electromagnetic transients in dispersive media. It considers propagation in water using Debye and composite Rocard-Powles-Lorentz models (Laurens and Oughstun 1999) for the complex permittivity. To avoid the problem mentioned above, standard filter design techniques are used to derive frequency domain filter transfer functions that are causal. The study addresses this question: For practical transmitted spectra, does precursor propagation provide any features that can be used to advantage over conventional signal propagation in models of dispersive media of interest? A companion experimental study is currently in progress that will attempt to measure the effects studied here.

The following sections discuss the calculational approach taken and the numerical results for Debye and Rocard-Powles-Lorentz models of electromagnetic transient propagation in water. The results indicate that for water using these models at UHF and below, precursors form at the leading and trailing edges of gated sinusoidal pulses. They are more strongly excited when the transient signal contains broadband energy at frequencies below the carrier. The energy in wideband signals including low frequency content decays algebraically with depth. The low frequency content does not need to include dc, but if it does not, a depth will be reached where the energy does decay exponentially. Narrowband signals decay exponentially with depth until the energy in the spectrum below the carrier begins to dominate the total energy. At that point, the behavior is that of the wideband signals discussed above.

Three points should be emphasized: 1. The rate of decay of energy with depth is important, but the actual value of energy remaining is more important. 2. As Roberts points out, real systems have a noise floor. If the energy that makes it through the medium is less than the noise spectral density, the signal is not useful (unless it can be coherently integrated over multiple pulses). 3. Since the media under consideration are linear (although dispersive), energy is not transferred from one part of the spectrum to another. For greatest penetration, the energy in the initial signal should be concentrated in the passband of the medium.

2.0 Calculational Approach

A dispersive dielectric is assumed to fill the half-space $x \geq 0$. The electric field to be propagated is calculated in the time domain at $x = 0$. It is assumed to exist within the dielectric medium — no reflection loss at the interface at $x = 0$ is included. Propagation of time-harmonic plane waves in the x-direction is given by the factor

$$e^{j(\omega t - k \cdot x)}$$

A well-known potential source of confusion is the difference between the physics and engineering literature in the form of the propagation factor. Many authors, especially in physics (eg. Jackson 1975), use the propagation factor

$$e^{i(k \cdot x - \omega t)}$$

This difference affects the expressions for the complex dielectric and propagation constants, frequency domain expressions for filter transfer functions, etc. In this report, I have converted all expressions to the $e^{j\omega t}$ time-harmonic convention.

2.1 Complex Relative Dielectric Permittivity and Wavenumber

For comparison with other studies, the dielectric is assumed to be water. Initially, the Debye model was used. The Debye model describes the rotational alignment of the dipole moments of the polar water molecules using one or more relaxation times. A conduction term has been added to the model to account for the conductivity of the water sample used. In this model, the relative complex dielectric permittivity is given by

$$\varepsilon_{rD} = \varepsilon_{r\infty} + \frac{\delta\varepsilon}{1 + j \cdot \omega\tau} - \frac{j \cdot \sigma_s}{\omega\varepsilon_0}$$

The dc to microwave response of water is well modeled by these parameters (Blaschak and Franzen 1995):

$\varepsilon_0 = 8.854 \cdot 10^{-12}$ F/m,
$\varepsilon_{r\infty} = 5.5$,
$\sigma_s = 1 \times 10^{-5}$ S,
$\tau = 8.1 \cdot 10^{-12}$ s, and
$\delta\varepsilon = 74.6$.

In the Lorentz model, the complex permittivity is given by (Oughstun and Sherman 1994)

$$\varepsilon_L = \varepsilon_0 \left(1 - \sum_j \frac{b_j^2}{\omega^2 - \omega_j^2 - 2j \cdot \delta_j \omega} \right)$$

The polarization resonances that the Lorentz model is normally applied to are typically electronic polarizations, which occur at infrared frequencies. They do not model the rotational resonances in the microwave range. Laurens and Oughstun (1999) publish the parameters for a composite Rocard-Powles-Lorentz model of triply distilled water. They model the rotational polarization component of the dispersion by a first-order correction to the Debye model known as the Rocard-Powles component. The resonance polarization component, important for frequencies above 10^{13} Hz, is accounted for by the Lorentz component of the model. Since the frequencies where the Lorentz component is important are so high compared to the frequencies of interest in this study, the results for the two models are expected to be very similar. In the composite model, the complex permittivity is given by (Laurens and Oughstun 1999)

$$\varepsilon_L = \varepsilon_\infty + \sum_{k=0,2} \frac{a_k}{(1 + j\omega\tau_k)(1 + j\omega\tau_{fk})} - \sum_{k=11,13,15,17} \frac{b_k^2}{\omega^2 - \omega_k^2 - 2j\delta_k\omega} - \frac{j \cdot \sigma_s}{\omega\varepsilon_0}$$

Again, a conductivity term has been added to their model, to better match the low frequency response of the deionized, but not triply distilled, water used in our measurements. In addition, a_0 in the composite model was increased from 74.1 to 76.1 to give a better match of the real part of the relative dielectric constant. An overlay of the real and imaginary parts of the complex permittivity shown in Figures 1 and 2 illustrate that the two models (as modified) are very similar in the frequency range of interest – microwaves and below. In the computations that follow, the only difference between the results for the two models was slightly higher attenuation for the composite model, especially at high frequencies. The results shown will be for the Debye model.

For both dielectric models, the complex wavenumber is computed as

$$k = \frac{\omega}{c} \sqrt{\varepsilon_r}$$

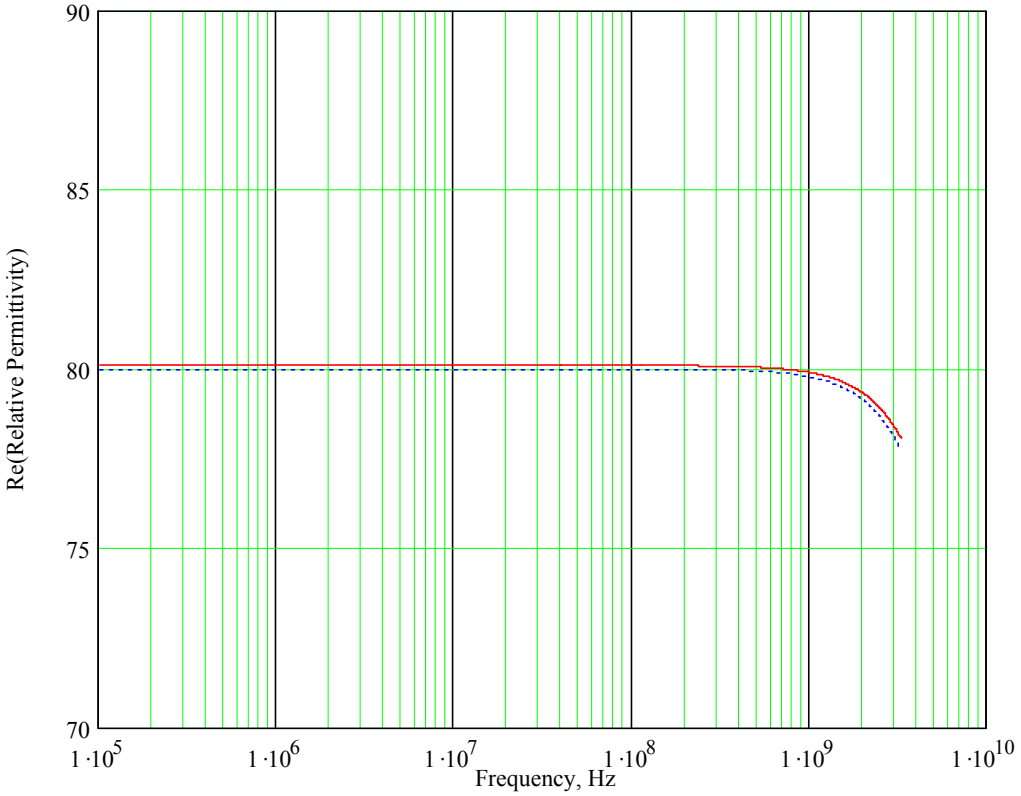

Figure 1. Real Part of Relative Dielectric Constant for Debye (solid) and Composite (dotted) Models.

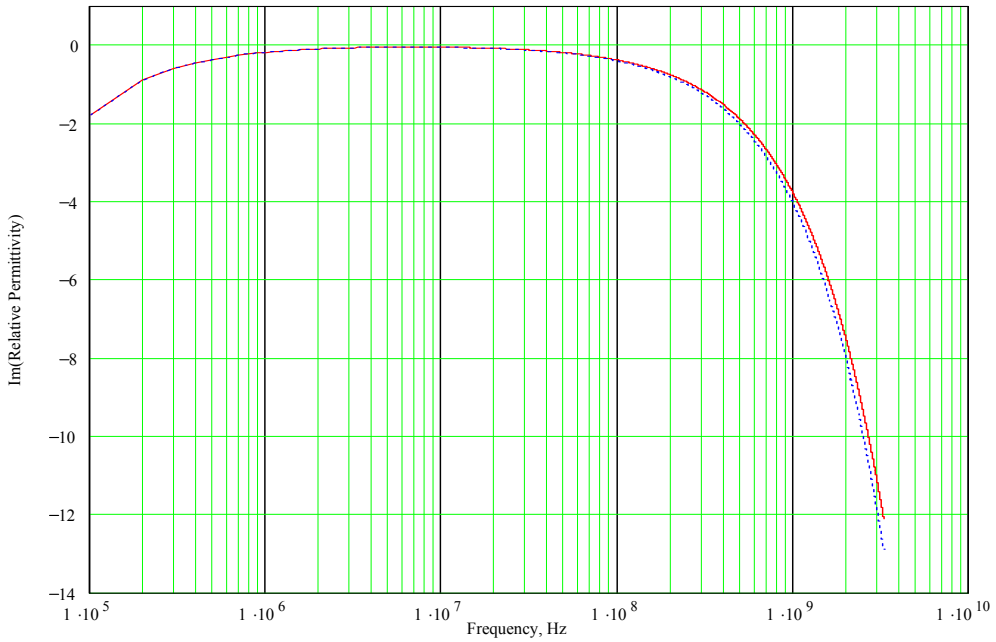

Figure 2. Imaginary Part of Relative Dielectric Constant for Debye (solid) and Composite (dotted) Models.

2.2 Filter Design

To obtain causal filter responses, standard analog filter design techniques were applied (Daryanani 1976). A Butterworth 3rd order low-pass prototype was chosen due to its reasonably well-behaved impulse response and good stopband performance. The lowpass prototype was then transformed into a bandpass filter with the desired band edges using the lowpass to bandpass transformation.

Two filter bandwidths were used in this study. The frequency responses of these filters are shown in Figure 3. The goal of using the filters was to limit the bandwidth of the signal propagating through the dielectric without appreciably changing the signal pulse shape. Thus, most of the pulse energy needed to lie within the filter bandwidth. Both filters were centered on 435 MHz. A 10 MHz wide filter simulates the bandwidth of a radar-like signal of pulse width τ of 100 ns or greater. A 200 MHz wide filter simulates the extent of frequency content of a wideband or ultrawideband (UWB) signal, assuming that the RF carrier is in the VHF or UHF bands. The 10 MHz wide filter was designed to have less than 0.5 dB loss in the passband of 430 to 440 MHz and greater than 20 dB loss below 415 MHz and above 455 MHz. It exceeded the design requirements. The 200 MHz filter was designed to have less than 0.5 dB loss in the passband of 335 to 535 MHz and greater than 20 dB loss below 232 MHz and above 770 MHz. It met the design requirements in the passband. The stopband attenuation was slightly low — 16.8 dB at both points. A higher order filter could achieve both design goals, but this filter's performance was considered adequate for the purpose of these calculations. The Appendix shows the frequency domain transfer function of both filters.

Figures 4 and 5 show the impulse responses of these two filters in the time domain. (The impulses occur at t = 10 ns so that the leading edge of their response could be seen clearly.) Note slow rise corresponding to their bandwidth, slight overshoot, and small after-ringing. The filters are causal with appropriate time delays. Their effect on the actual probe signals used in the study will be shown in the next section.

To address some of the concerns about low frequency content mentioned by Roberts (2002), it is desirable to have the same behavior in the simulation as frequency approaches zero as one would expect from a signal radiated from a realistic airborne antenna (Yaghjian 2003). Low frequency content depends upon the output spectrum of the transmitter and the ability of the antenna to radiate the longer wavelengths. Unless the transmitter is intended for ultrawideband operation (Taylor 1995), frequency content both above and below band will be suppressed by design. If nothing else, the transmitter output power spectrum falls off at least as $\omega^2 = (2\pi f)^2$ for $\omega \rightarrow 0$ if the stages are ac coupled. All antennas become electrically small at some point as frequency decreases. An antenna is considered electrically small when it can be contained in a sphere of radius $a = \lambda/2\pi$ (Wheeler 1975). The limitations and behavior of small antennas have been studied extensively (Wheeler 1975; Hansen 1981; Wheeler 1983; Wheeler 1984; McLean 1996). The power radiated by a small antenna falls off as ω^3 for $\omega \rightarrow 0$.

Since the pulse width of the gated sinusoids used in this study are not constrained to be an integral number of periods of the carrier, the unfiltered probe signals may have a dc component. For carriers widely separated from zero frequency in terms of the reciprocal of the pulse width, this component will be small compared to frequencies near the carrier. The filtered probe signals have had this component removed. As can be seen from the expressions for the filter transfer functions, both filters fall off as ω^3 for $\omega \rightarrow 0$.

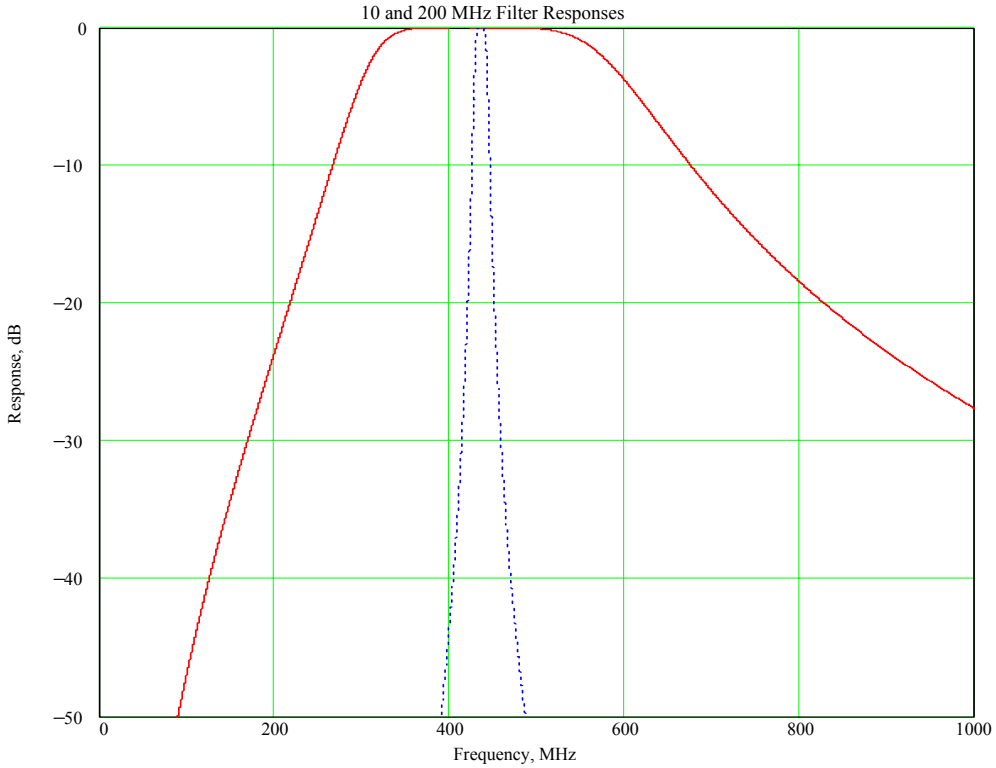

Figure 3. 10 MHz (dotted) and 200 MHz (solid) Bandpass Filter Frequency Responses

An equal delay filter, such as the Bessel filter approximation, is potentially better than the Butterworth filter in this application; performance in the stopband is not as good, but the equal delay of frequency components in the passband and especially in the transition band would minimize distortion of the dispersed pulse shape (Blinchikoff and Zverev 1976). In addition, a digital filter implementation could be used rather than simply calculating an analog transfer function. Future work may explore the use of these filters.

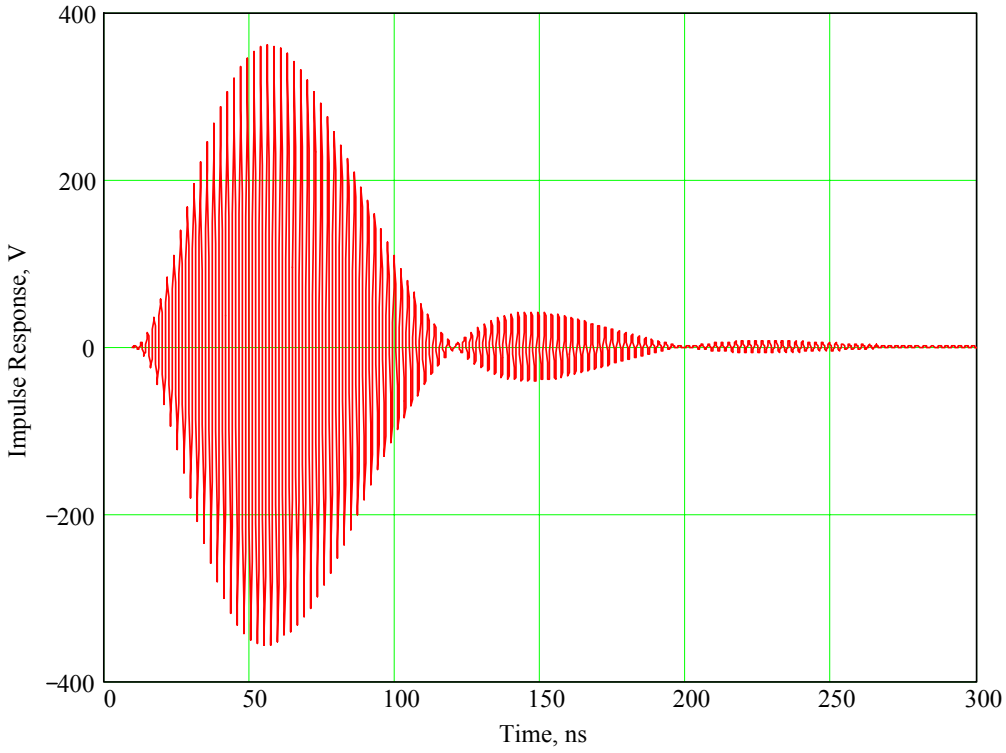

Figure 4. Impulse response of 10 MHz wide filter.

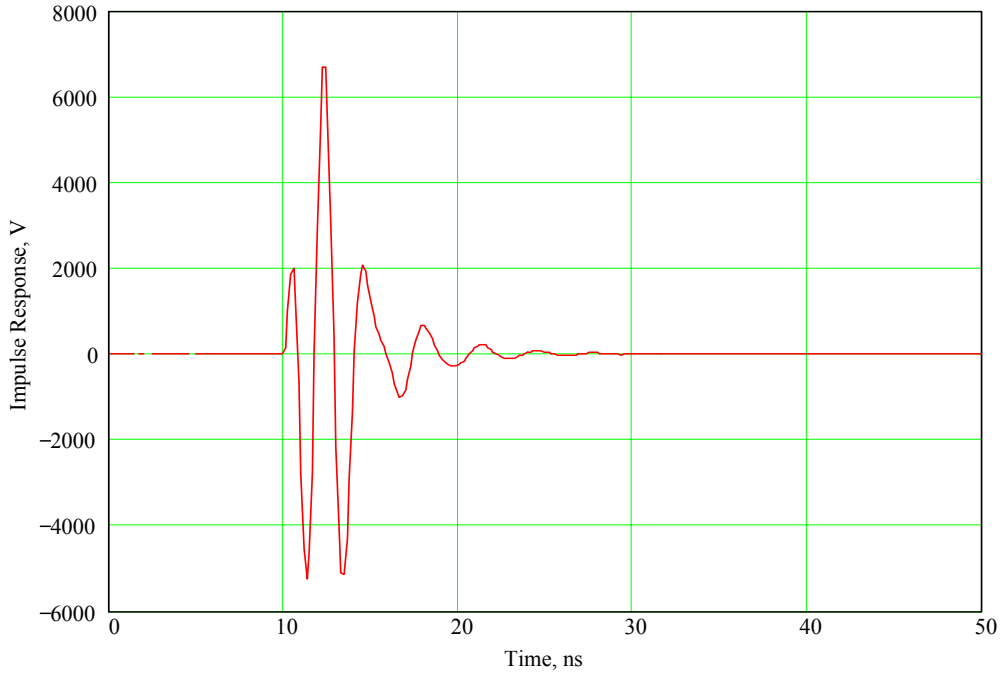

Figure 5. Impulse Response of 200 MHz wide filter

3.0 Results

3.1 Probe Signals

Two different signals were used to probe the response of the dielectric, corresponding to the two filter bandwidths. The signals were gated sinusoids — an RF carrier turned on at the beginning of the pulse and turned off at the end. The phase of the gated signal was not synchronous with the gate — the filter provides smoothing of the waveform at these points. The RF carrier frequency was chosen to be 435 MHz, at the center of both filter passbands. The long pulsewidth was chosen to be 1 μs. Most of its energy is contained within a 1 MHz bandwidth, so the 10 MHz filter has little effect on its pulse shape. The short pulsewidth was 10 ns long. Most of its energy was contained within a 100 MHz bandwidth. The 200 MHz filter changed its shape slightly. Figures 6 and 7 show the effect of the filters alone on the gated carriers. In all of the following figures, the ordinate is time in microseconds, and the abscissa is the signal amplitude. The amplitude can be considered to be volts in a water-filled TEM transmission line, or volts per meter in water with a propagating TEM wave, unless otherwise noted.

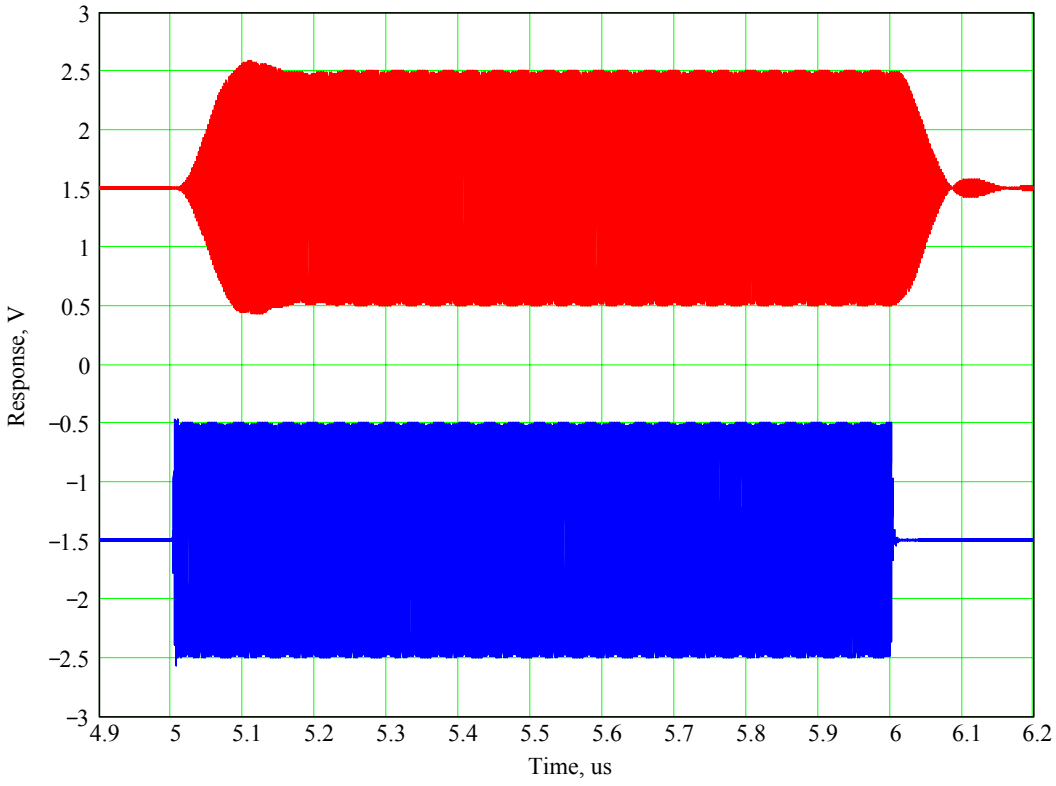

Figure 6. 1 us signal filtered by 10 MHz (upper) and 200 MHz (lower) filters. Waveforms are offset by +/- 1.5 V.

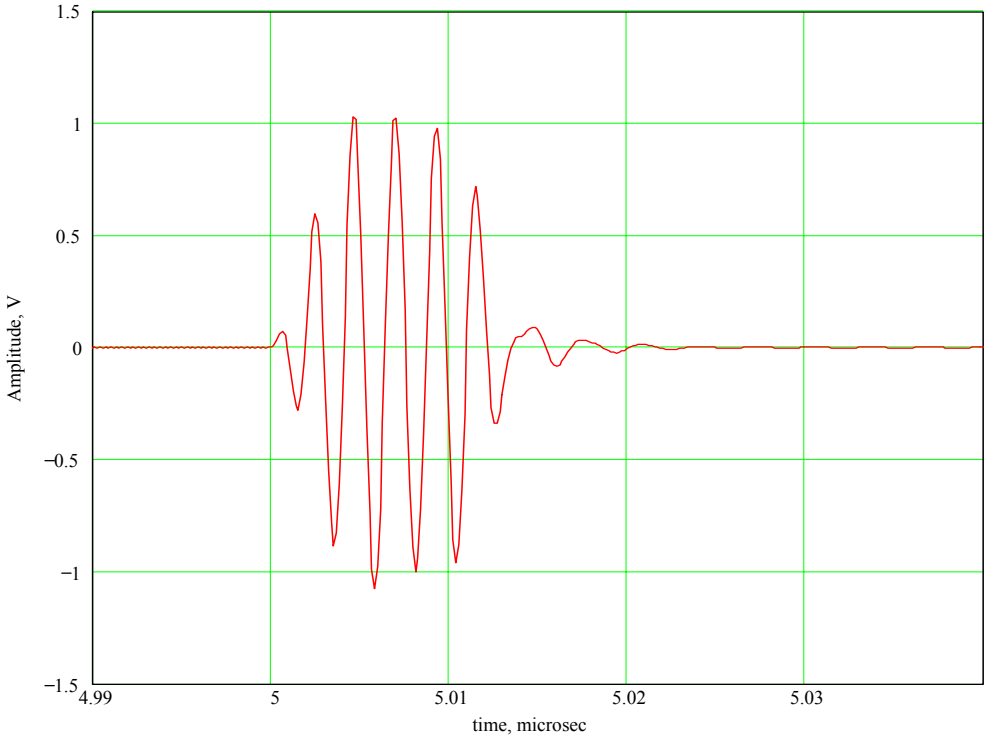

Figure 7. 10 ns signal filtered by 200 MHz filter.

3.2 Pulse Shapes at Various Depths

Because the frequency components of the gated sinusoids travel at different velocities and are attenuated at different rates as they penetrate the medium, the pulse shape changes with depth. Figure 8 and Figure 9 show the leading edges of the 1 μs signal at depths of 1, 3, and 5 m in water, and Figure 10 shows the trailing edges. The lower sidebands of these signals contain energy that becomes an increasingly larger fraction of the total as depth increases. This is why the overshoot at the leading edge and the undershoot at the trailing edge increase as depth increases. (These signals also contain a small dc component, and, thus, could not be radiated exactly as shown. They are plotted for comparison with the following filtered results.) Analogous 10 MHz wide filtered signals are shown in Figure 11, Figure 12 and Figure 14. Precursors, although present, are not apparent on this scale, since the filter attenuates the low frequency energy that produces them relative to the main signal carrier. Figure 13 overlays the filtered and unfiltered leading edges at 5 m depth for comparison.

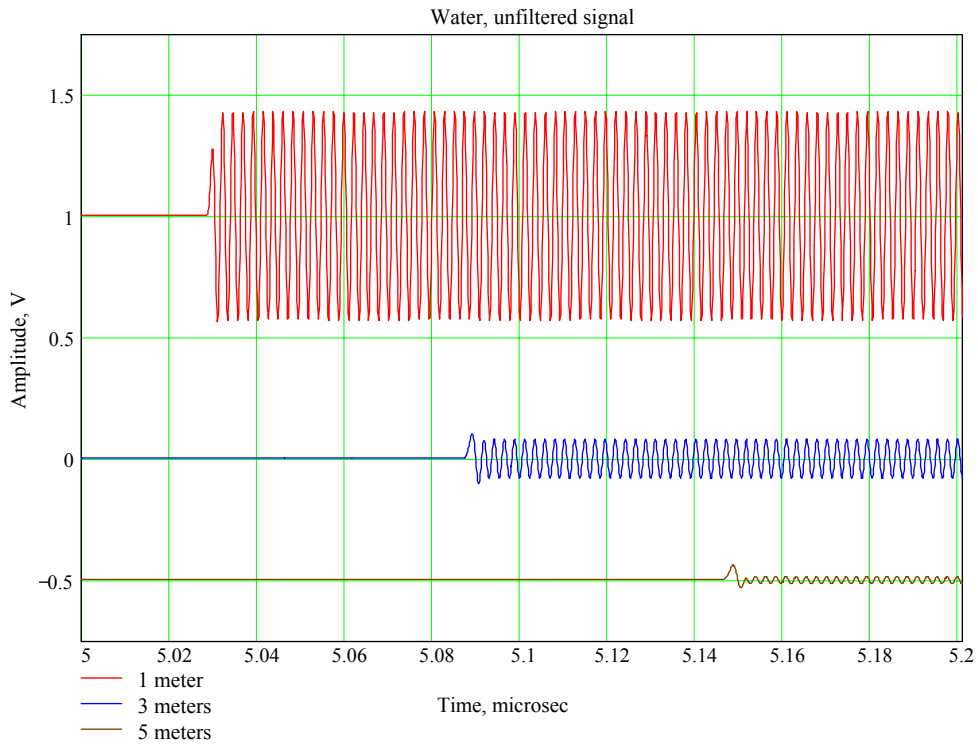

Figure 8. Leading edge of unfiltered 1 us signal at various depths. Baselines offset for clarity.

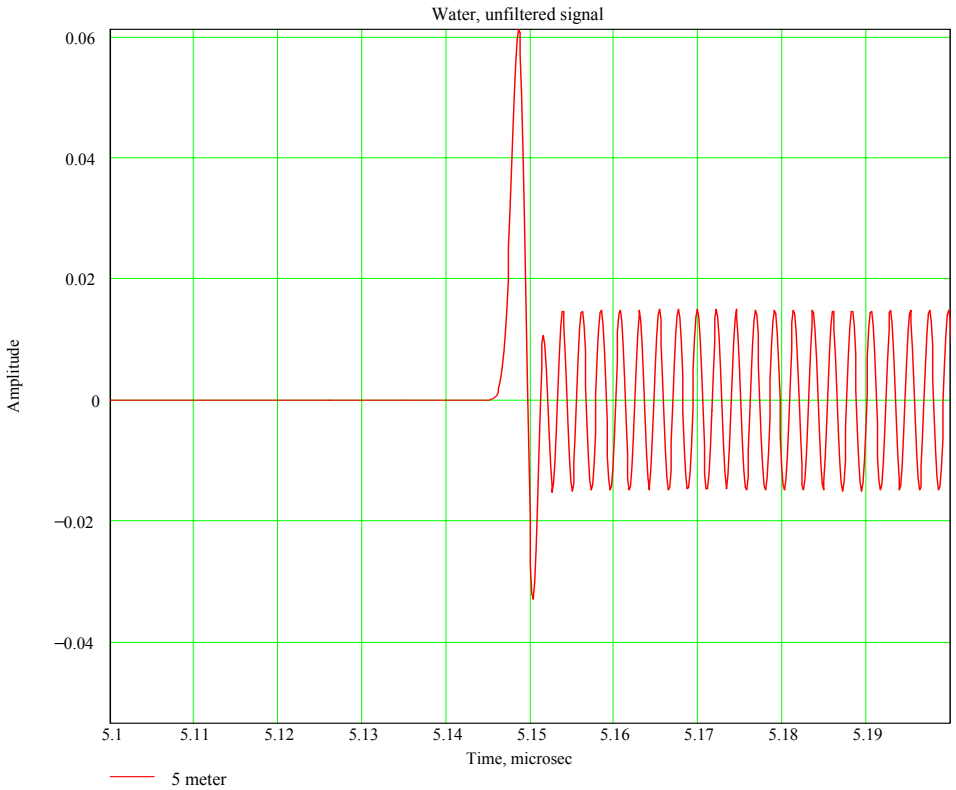

Figure 9. Closeup of leading edge of unfiltered signal at 5 m depth.

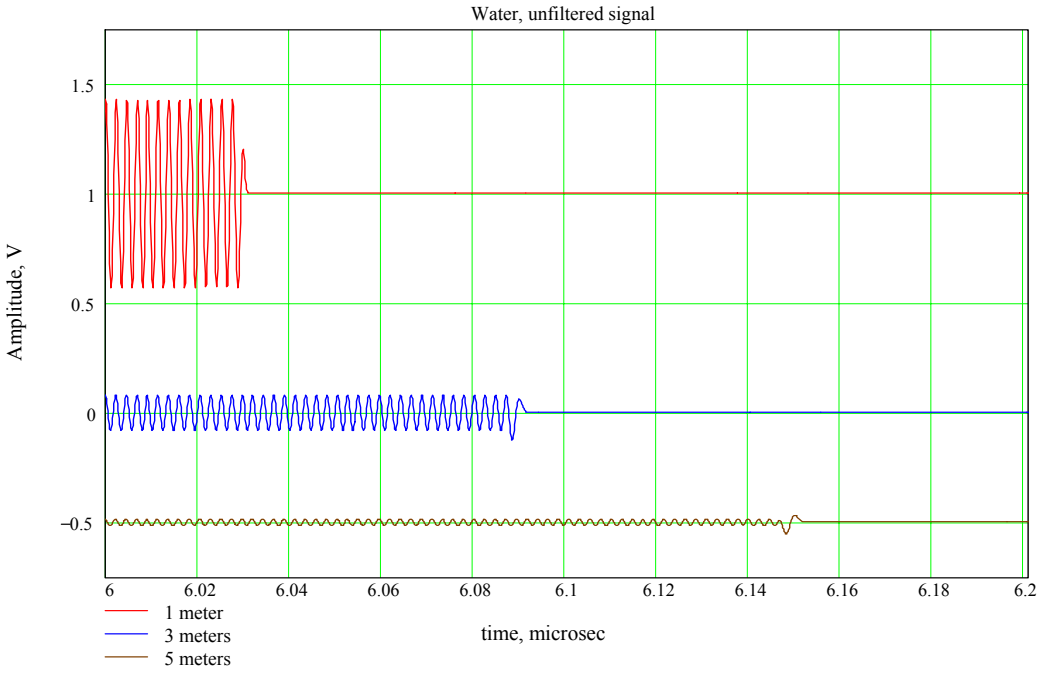

Figure 10. Trailing edge of unfiltered 1 us signal. Baselines offset for clarity.

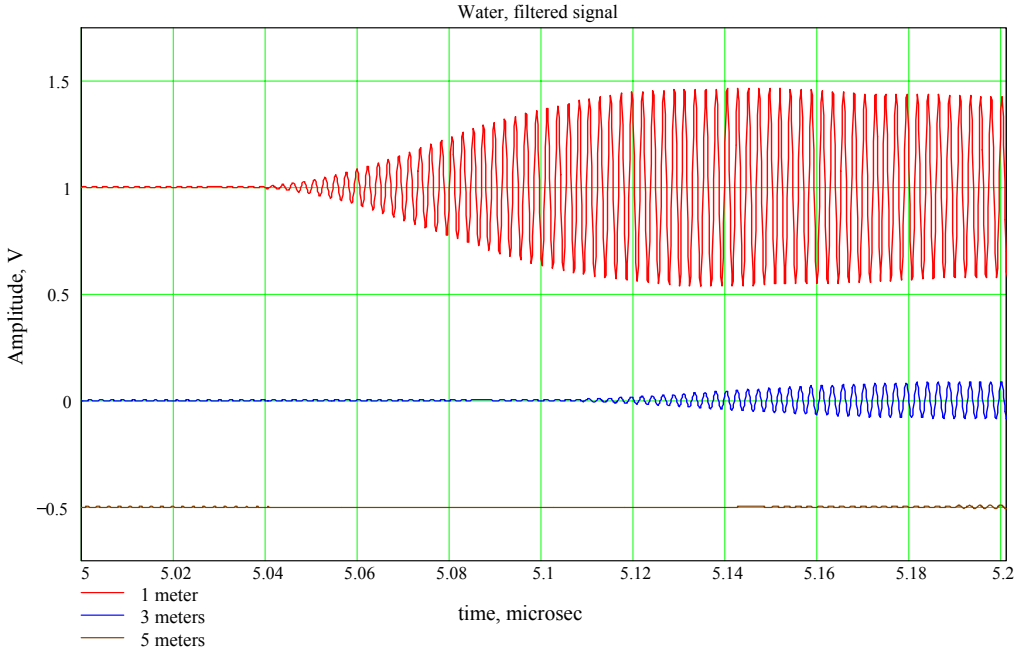

Figure 11. Leading edge of filtered 1 us signal at various depths. Baselines offset for clarity.

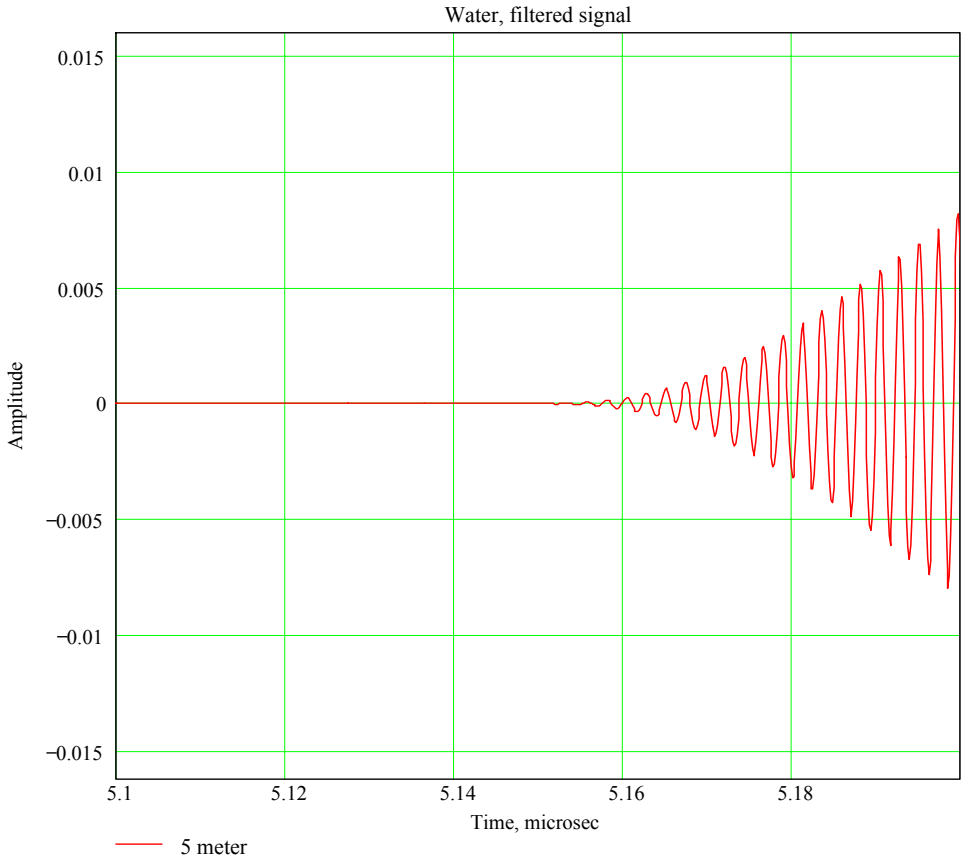

Figure 12. Closeup of leading edge of filtered signal at 5 m depth.

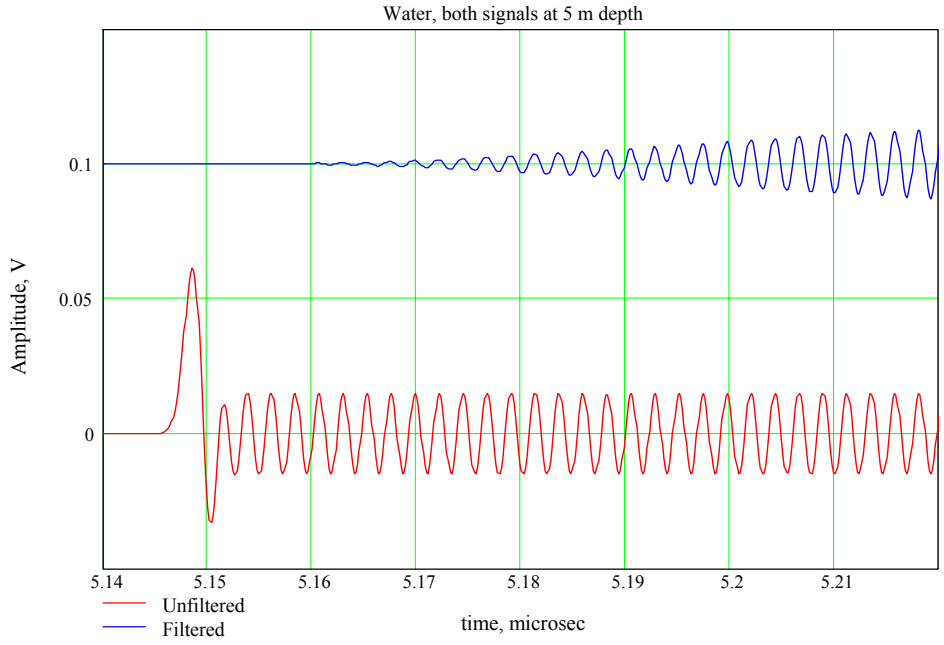

Figure 13. Comparison of filtered and unfiltered signals at 5 m depth. Baselines shifted for clarity.

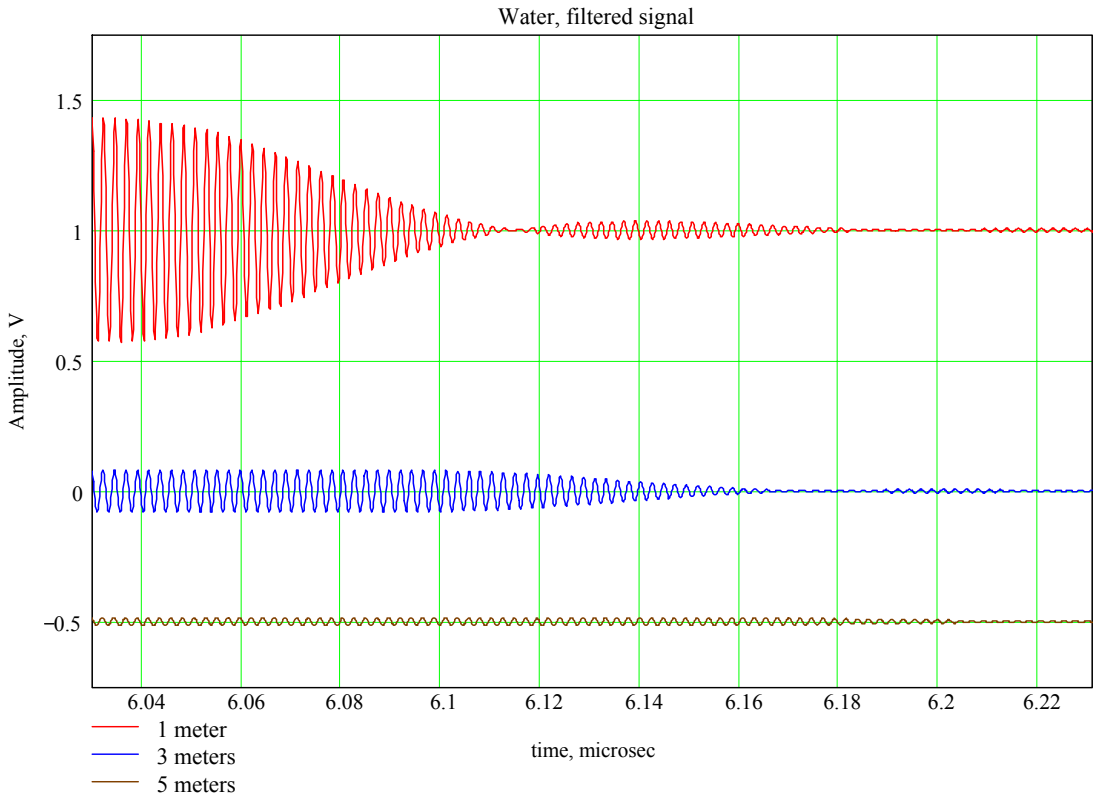

Figure 14. Trailing edge of filtered 1 us signal. Baselines offset for clarity.

Figure 15 shows the leading edge of the filtered signal after it has penetrated to a depth of 20 m. The precursor is clearly visible, but its peak field value is extremely low – approximately $1.5 \cdot 10^{-8}$ V/m. The pulse eventually reaches a steady value of $5 \cdot 10^{-8}$ V/m. Notice that the period of oscillation of the precursor is longer than the driven oscillations at the carrier frequency later in the pulse. At 40 m, as shown in Figure 16 the carrier has disappeared, leaving only precursors at the leading and trailing edges. Again, these signals are at extremely low amplitude compared to the initial incident signal. No attempt was made here to include realistic noise levels, although that could certainly be done given the properties of the specific receiving system and noise environment.

Figures 17 through 20 show similar results for the unfiltered and 200 MHz wide filtered 10 ns pulse. In this case, the leading and trailing edges are both visible on the same plot.

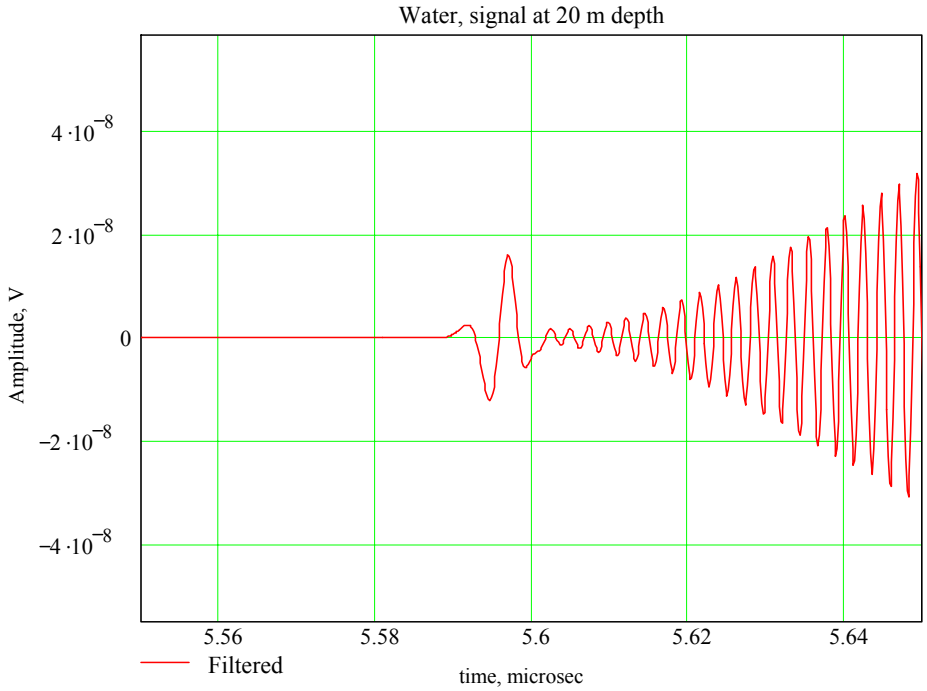

Figure 15. Precursor on filtered signal at 20 m depth.

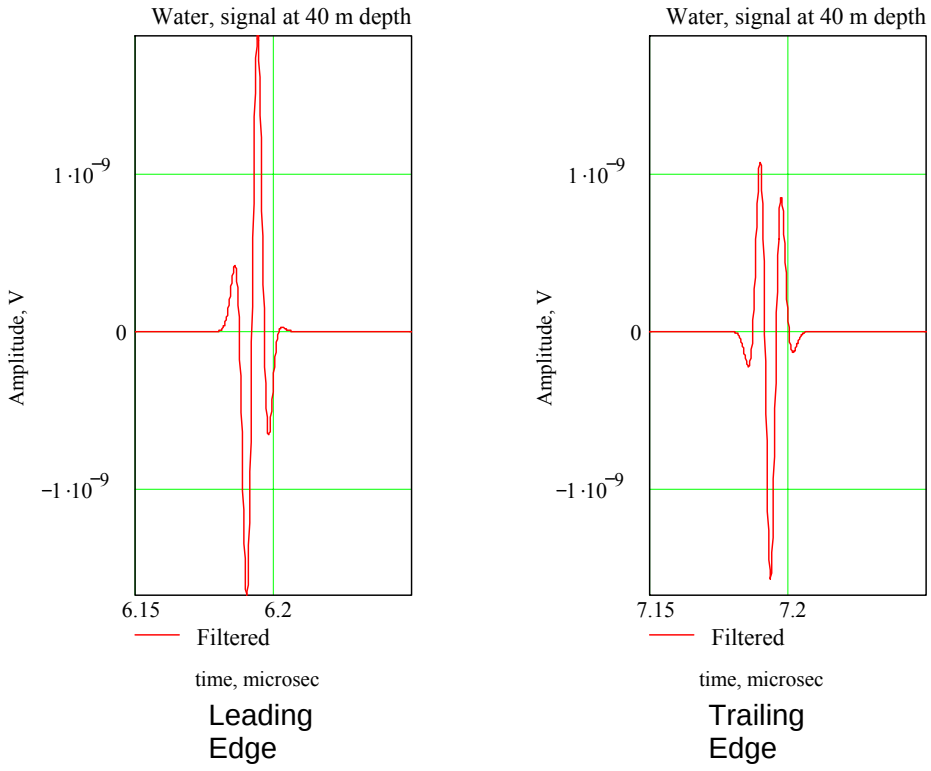

Figure 16. At 40 m, carrier has disappeared, leaving only precursors at leading and trailing edges.

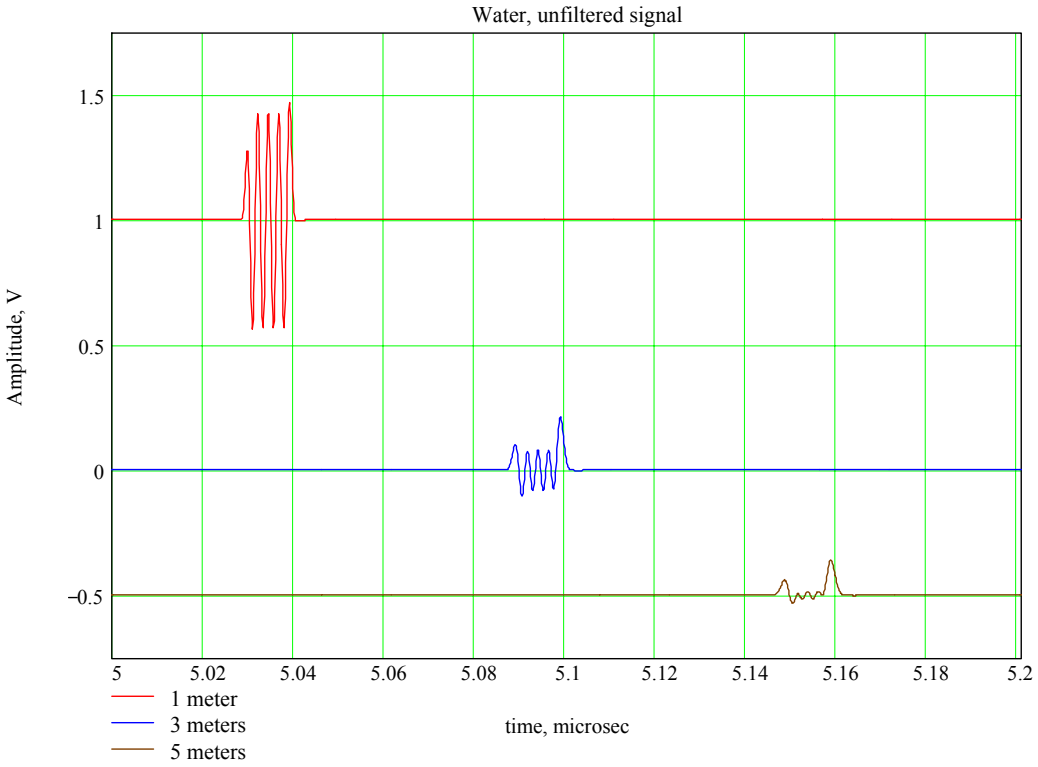

Figure 17. Unfiltered 10 ns signal at various depths. Baselines offset for clarity.

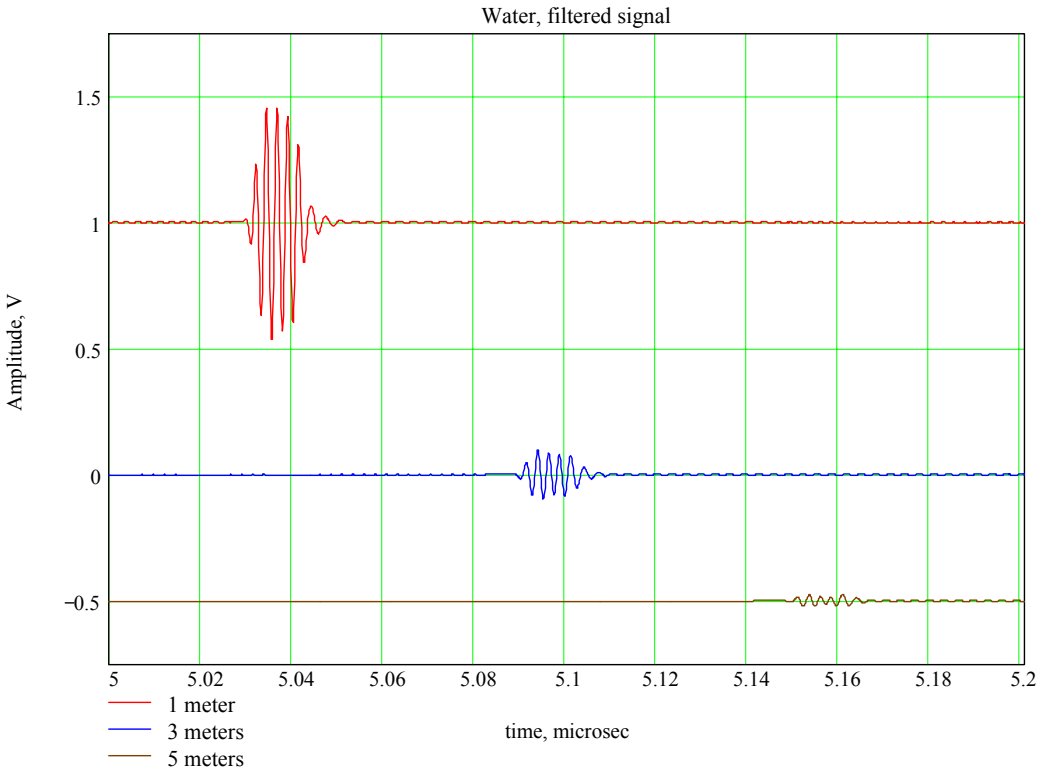

Figure 18. Filtered 10 ns signal at various depths. Baselines offset for clarity.

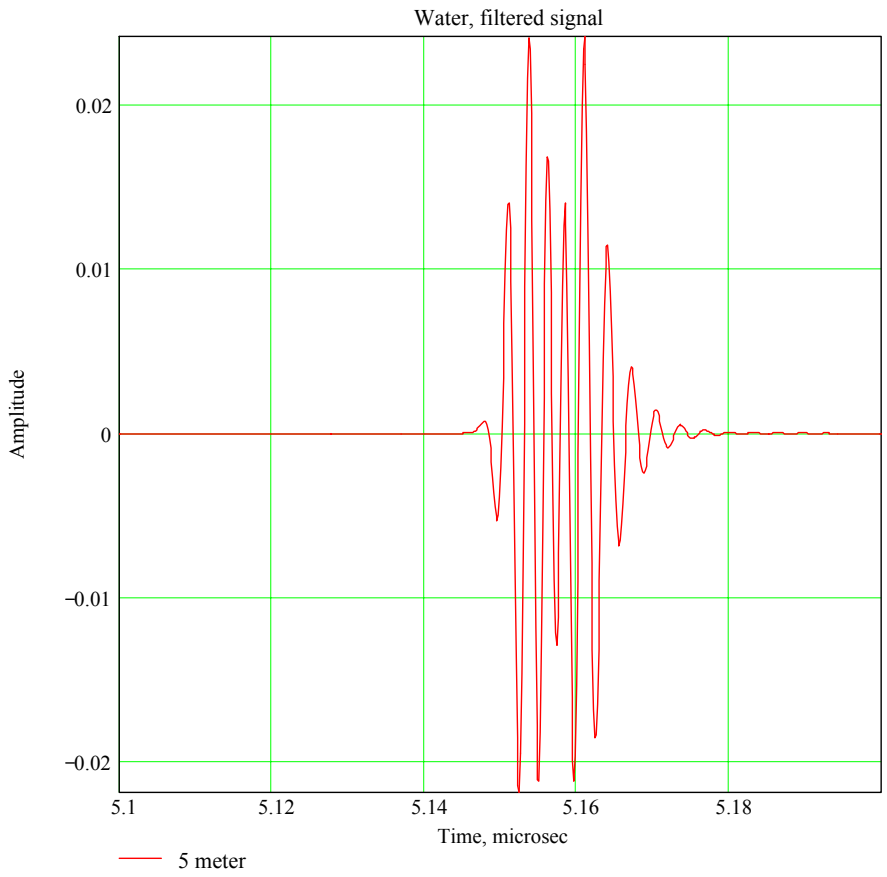

Figure 19. Closeup of 10 ns filtered pulse at 5 m depth.

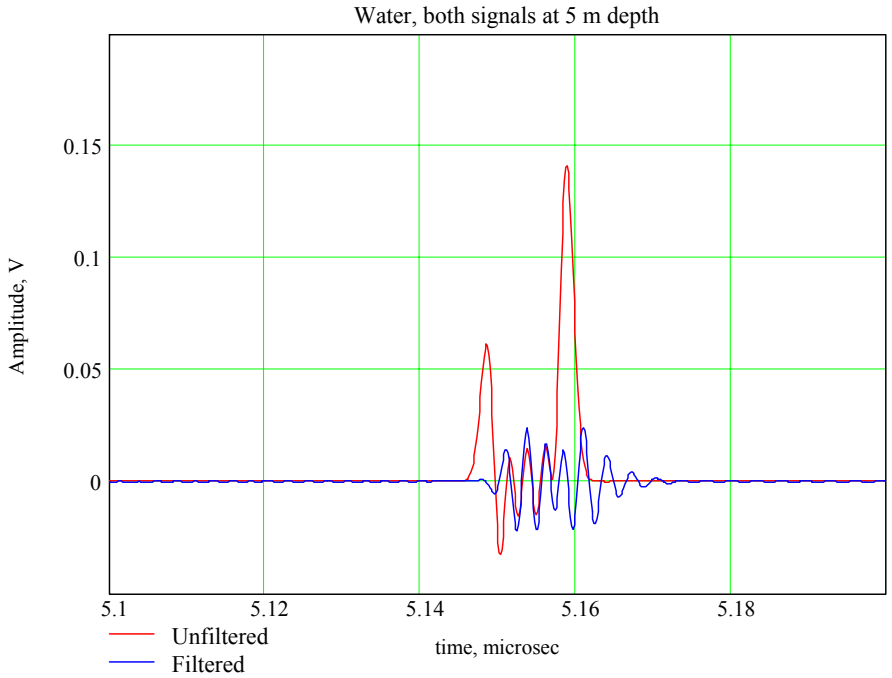

Figure 20. Overlay of filtered and unfiltered 10 ns pulses as 5 m depth.

3.3 Energy Decay with Depth

A function proportional to the total energy in the pulse versus depth can be calculated by summing the squared amplitudes of the frequency components at each depth. By Parseval's theorem, this is the same as integrating the squared voltage as a function of time — the energy delivered to a 1-Ω resistor. This is sometimes called the 1-Ω energy.

For the calculation of energy decay with depth, a third probe signal was used in addition to the two gated sinusoids discussed above. A unit impulse was synthesized in the frequency domain by assigning each frequency component the value 1 + j0, times a linear phase shift $\exp(-j\omega t_d)$ to add a time delay t_d. This signal cannot be radiated, of course, but it illustrates the $x^{-1/2}$ depth dependence. Two curves overlay in Figure 21: The calculated relative energy decay (solid), and an $x^{-1/2}$ curve fit. The agreement is excellent.

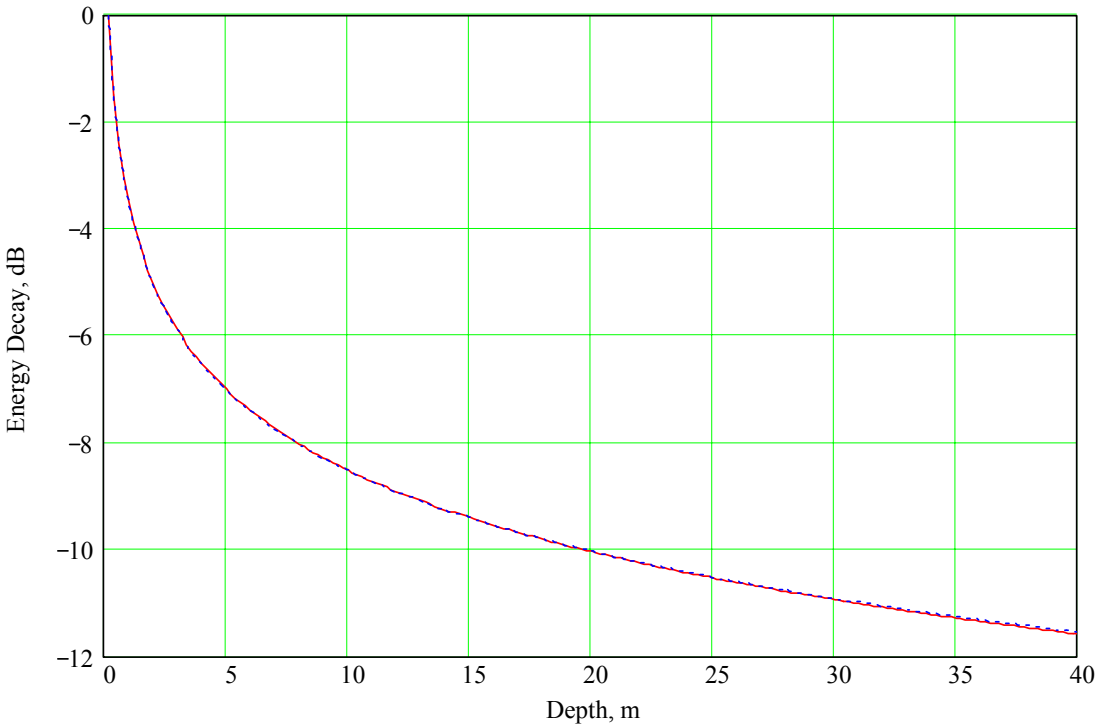

Figure 21. Decay of 1-Ohm Energy of Unit Impulse.

The 1-μs pulse is quite narrow band compared with the frequency dependence of the propagation factor. Thus, we would expect the energy decay with depth to be exponential — a straight line when plotted in dB — until the energy in the main spectral lobe becomes attenuated when compared to the low frequency sidelobes. At this point, the signal looks broadband, although it has been attenuated to a low level. Figure 22 illustrates the process. The attenuation is quite linear in dB (exponential in ratio) down to about 45 dB at 6 m depth. The rate of decay then slows considerably, reaching only 56 dB at 20 m. Figure 24 shows the spectrum at 8.5 m depth, near the knee of the curve. Because of the low-pass nature of the medium, the low frequency amplitudes are now comparable to the main signal. The energy content at low frequencies, that is, the integral

with frequency, is now higher since they occupy a broad spectral region at comparable amplitude. Thus, the low frequencies, with their lower attenuation, begin to dominate the response.

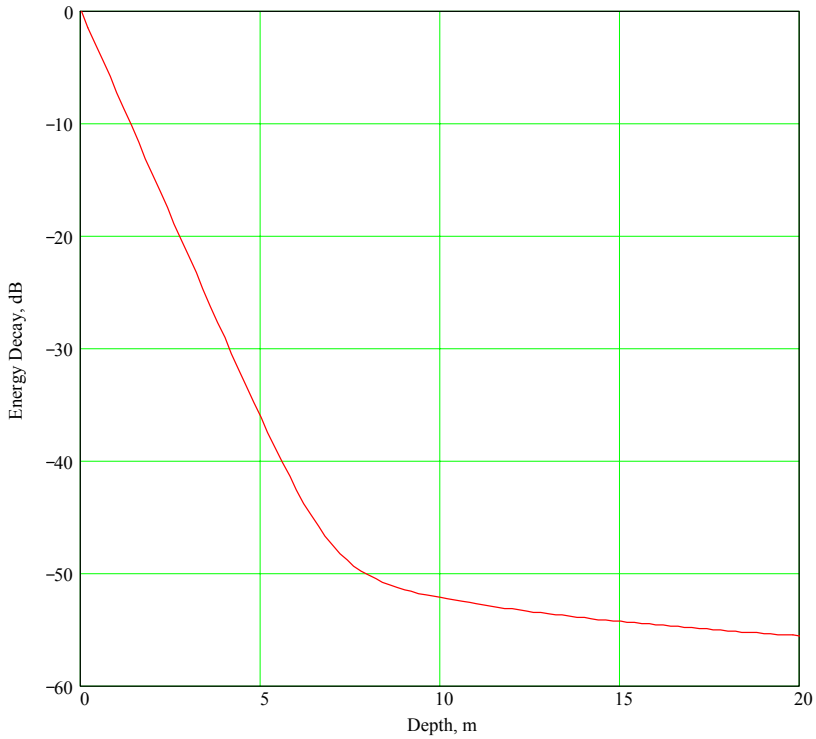

Figure 22. Energy Decay of 1 us signal, no filtering.

Figure 23 shows the same plot for the unfiltered 10 ns signal. The knee of this curve occurs at a lower attenuation and shallower depth, since the signal is more broadband to start with.

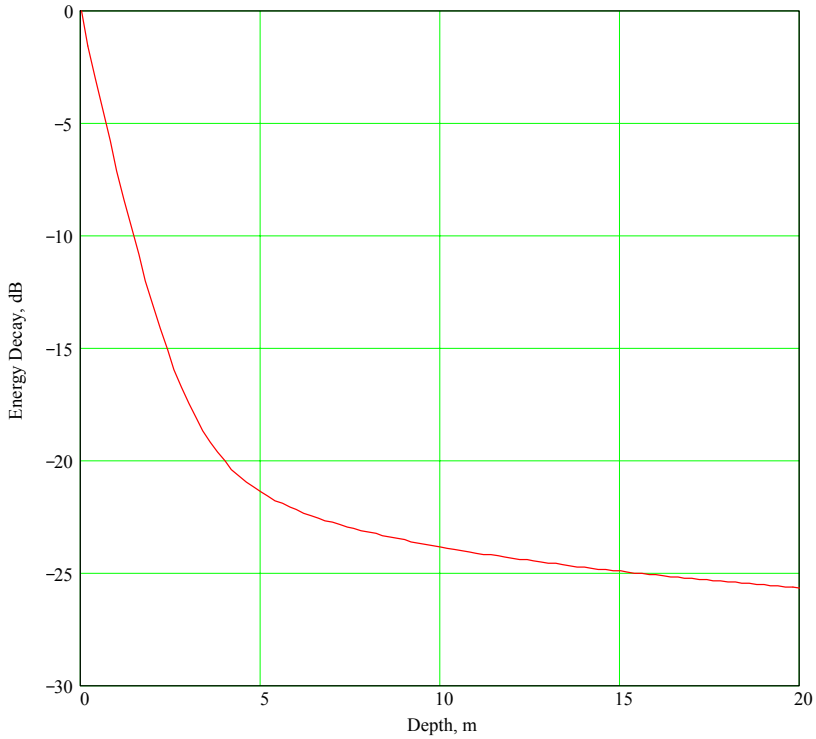

Figure 23. Energy Decay of 10 ns signal, no filtering.

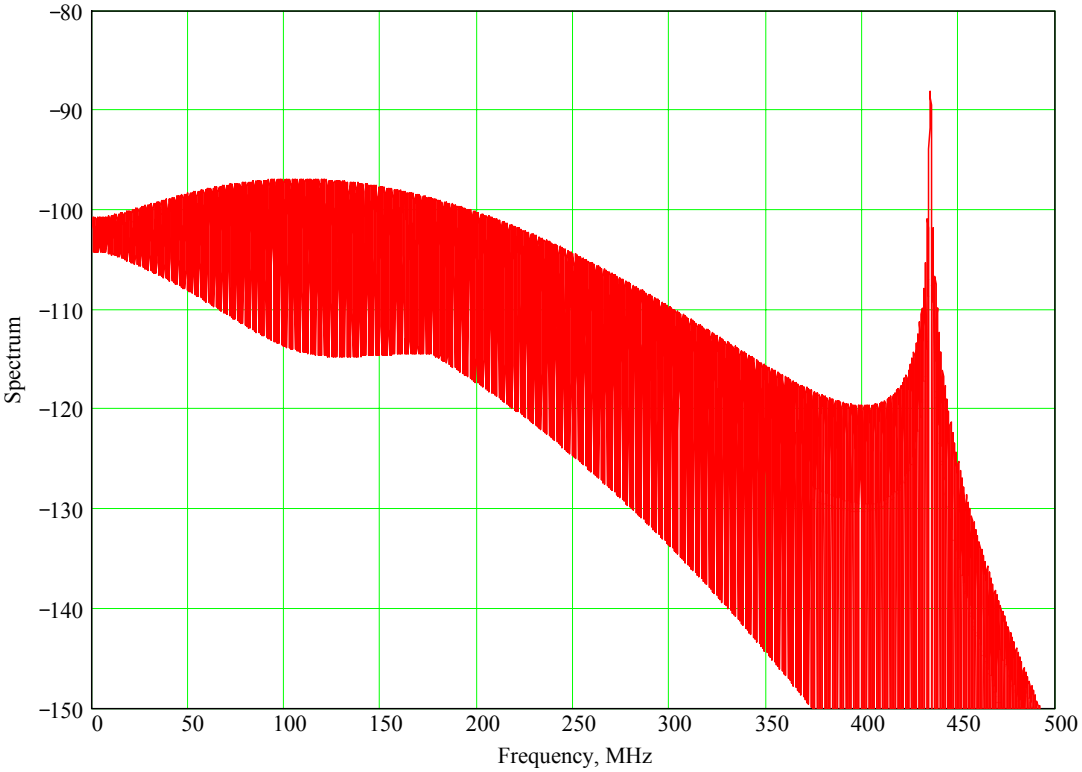

Figure 24. Spectrum of unfiltered 1 us pulse at 8.5 m depth.

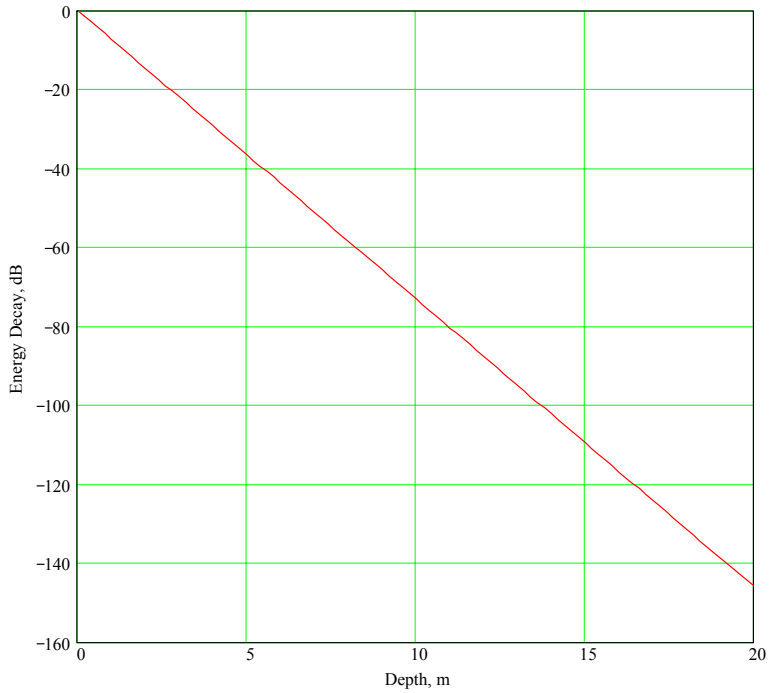

Figure 25. Energy Decay of 1 us signal, with 10 MHz filtering.

Notice in Figure 25, which is the 1 μs signal filtered by the 10 MHz bandpass filter, that the energy decay remains exponential, rather than algebraic, down to 20 m depth. Because of the filtering before propagation, the low frequency sidelobes have been supressed relative to the mainlobe at 435 MHz. Figure 26 shows the spectrum at the same depth and on the same scale as the unfiltered signal spectrum of Figure 24.

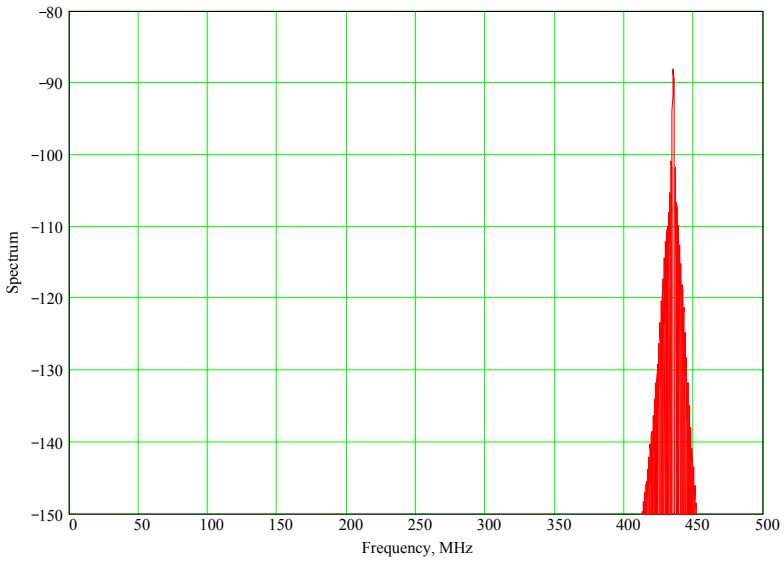

Figure 26. Spectrum of 10 MHz filtered 1 us pulse at 8.5 m depth.

4.0 Summary and Suggestions for Further Work

This study investigated the propagation of electromagnetic transients in dispersive media numerically. It considered propagation in water using Debye and composite Rocard-Powles-Lorentz models for the complex permittivity. In the microwave region and below, these models gave results that were both qualitatively and quantitatively similar. Standard filter design techniques were used to derive frequency domain filter transfer functions that were causal in order to avoid obscuring precursors due to the media by filter precursors.

The results indicate that for water using these models with signals at UHF and below, precursors form at the leading and trailing edges of gated sinusoidal pulses. They are more strongly excited when the transient signal contains broadband energy at frequencies below the carrier. The energy in wideband signals including low frequency content decays algebraically with depth. The low frequency content does not need to include dc, but if it does not, a depth will be reached where the energy does decay exponentially. Narrowband signals decay exponentially with depth until the energy in the spectrum below the carrier begins to dominate the total energy. At that point, the behavior is that of the wideband signals discussed above.

Three points should be emphasized: 1. The rate of decay of energy with depth is important, but the actual value of energy remaining is more important. 2. As Roberts points out, real systems have a noise floor. If the energy that makes it through the medium is less than the noise spectral density, the signal is not useful (unless it can be coherently integrated over multiple pulses). 3. Since the media under consideration are linear (although dispersive), energy is not transferred from one part of the spectrum to another. For greatest penetration, the energy in the initial signal should be concentrated in the passband of the medium.

Further work could usefully include equal-delay filters to reduce distortion of the transient pulse, especially in the transition band. The filters used in this work, although causal and designed so that most of the energy was in the passband, did distort the probe signals slightly, as shown in Figures 6 and 7. As models for heterogeneous materials become available, transient propagation through these materials could be predicted. Finally, detection limits could be predicted by adding the appropriate noise levels to the calculated voltages.

Appendix

200 MHz Filter transfer function:

$$H_{Butterworth_{jj}} := \frac{0.49223130 \cdot 10^{30} \cdot 1j \cdot (freq_{jj})^3}{\left[\left[27.792807 \cdot (freq_{jj})^2 - 0.78956836 \cdot 10^{10} \cdot 1j \cdot freq_{jj} - 0.49811657 \cdot 10^{19}\right] \cdot \left[772.44011 \cdot (freq_{jj})^4 - 0.21944321 \cdot 10^{12} \cdot 1j \cdot (freq_{jj})^3 - 0.33922297 \cdot 10^{21} \cdot (freq_{jj})^2 + 0.3932709 \cdot 10^{29} \cdot 1j \cdot freq_{jj} + 0.24812011 \cdot 10^{38}\right]\right]}$$

10 MHz Filter transfer function

$$H_{Butterworth_{jj}} := \frac{0.61528911 \cdot 10^{26} \cdot 1j \cdot (freq_{jj})^3}{\left[\left[27.792807 \cdot (freq_{jj})^2 - 0.39478419 \cdot 10^{9} \cdot 1j \cdot freq_{jj} - 0.52583989 \cdot 10^{19}\right] \cdot \left[772.44011 \cdot (freq_{jj})^4 - 0.10972161 \cdot 10^{11} \cdot 1j \cdot (freq_{jj})^3 - 0.29244718 \cdot 10^{21} \cdot (freq_{jj})^2 + 0.20759327 \cdot 10^{28} \cdot 1j \cdot freq_{jj} + 0.27650759 \cdot 10^{38}\right]\right]}$$

REFERENCES AND BIBLIOGRAPHY

Blaschak, J. and J. Franzen (1995). "Precursor Propagation in Dispersive Media from Short-Rise-Time Pulses at Oblique-Incidence." JOURNAL OF THE OPTICAL SOCIETY OF AMERICA A-OPTICS IMAGE SCIENCE AND VISION **12**(7): 1501-1512.

Blinchikoff, H. J. and A. I. Zverev (1976). Filtering in the Time and Frequency Domains. New York, New York, John Wiley and Sons.

Brock, B. C. and W. E. Patitz (1993). Factors governing selection of operating frequency for subsurface-imaging synthetic-aperture radar. Albuquerque, NM. Sandia National Laboratories. SAND93-2010C.

Daryanani, G. (1976). Principles of Active Network Synthesis and Design. New York, New York, John Wiley and Sons.

Hansen, R. C. (1981). "Fundamental Limitations in Antennas." Proceedings of the IEEE **69**(2): 170-182.

Jackson, J. D. (1975). Classical Electrodynamics. New York, New York, John Wiley and Sons.

Laurens, J. E. K. and K. E. Oughstun (1999). Electromagnetic Impulse Response of Triply-Distilled Water. Ultra-Wideband, Short-Pulse Electromagnetics 4. E. Heyman, Benjamin Mandelbaum and Joseph Shiloh. New York, New York, Kluwer Academic/Plenum**:** 458.

Loubriel, G. M., F. J. Zutavern, et al. (1994). Transmitters for ground- and foliage-penetrating impulse radar. Albuquerque, NM. Sandia National Laboratories. SAND93-2829.

McLean, J. S. (1996). "A Re-Examination of the Fundamental Limits on the Radiation Q of Electrically Small Antennas." IEEE Transactions on Antennas and Propagation **44**(5): 672-676.

Oughstun, K. E. and G. C. Sherman (1994). Electromagnetic Pulse Propagation in Causal Dielectrics. Berlin, Springer-Verlag.

Roberts, T. M. (2002). "Radiated pulses decay exponentially in materials in the far fields of antennas." Electronics Letters **38**(14): 679-680.

Taylor, J. D., Ed. (1995). Introduction to Ultra-Wideband Radar Systems. Boca Raton, Florida, CRC Press.

Wheeler, H. A. (1975). "Small Antennas." IEEE Transactions on Antennas and Propagation **AP-23**(4): 462-469.

Wheeler, H. A. (1983). "The Wide-Band Matching Area for a Small Antenna." IEEE Transactions on Antennas and Propagation **AP-31**(2): 364-367.

Wheeler, H. A. (1984). Small Antennas. Antenna Engineering Handbook. H. Jasik. New York, New York, McGraw-Hill**:** 6-1 : 6-18.

Yaghjian, A. D. (2003). Personal Communication.

DISTRIBUTION

Internal Distribution:

1	MS	1165	William Guyton, 15300
1		1153	Malcolm Buttram, 15330-1
1		1153	Guillermo Loubriel, 15333
50		1153	Larry Bacon, 15333
1		1153	Alan Mar, 15333
1		1153	Larry Rinehart, 15333
1		1153	Fred Zutavern, 15333
1		1153	Dale Coleman, 15331
1		1153	Steven Dron, 15336
1		1153	Robert A. Salazar 15333
1		1153	Luis L. Molina 15333
1		1193	Jane M. Lehr 01645

1	MS	9018	Central Technical Files, 8945-1
2		0899	Technical Library, 9616